Articles

Solution Structure of P05-NH_2, a Scorpion Toxin Analog with High Affinity for the Apamin-Sensitive Potassium Channel‡

S. Meunier,§ J.-M. Bernassau,‖ J.-M. Sabatier,⊥ M. F. Martin-Eauclaire,⊥ J. Van Rietschoten,⊥ C. Cambillau,§ and H. Darbon*,§

Faculté de Médecine-Nord, LCCMB, CNRS URA 1296, Boulevard Pierre-Dramard, 13916, Marseille Cedex 20, Sanofi-Recherche, 371, rue du Pr. Joseph-Blayac, 34184 Montpellier Cedex 04, and Faculté de Médecine-Nord, CNRS URA 1455, Boulevard Pierre-Dramard, 13916, Marseille Cedex 20, France

Received April 30, 1993; Revised Manuscript Received July 6, 1993•

ABSTRACT: The venom of the scorpion *Androctonus mauretanicus mauretanicus* contains a toxin—P05—which is structurally and functionally similar to scorpion leiurotoxin I (87% sequence identity), a blocker of the apamin-sensitive Ca^{2+}-activated K^+ channels. P05, a 31-residue polypeptide cross-linked by three disulfide bridges, also possesses binding and physiological properties similar to those of the bee venom toxin apamin (18 residues, two disulfides). However, the amino acid sequences of these two polypeptides are dissimilar, except for a common Arg-Arg-Cys-Gln motif which is located on an α-helix. P05-NH_2, a synthetic analog of P05, unlike native P05, was found to bind irreversibly to the apamin receptor. The solution structure of P05-NH_2 has been solved by conventional two-dimensional NMR techniques followed by distance geometry and energy minimization. The obtained conformation is composed of two and an half turns of α-helix (residues 5–14) connected by a tight turn to a two-stranded antiparallel β-sheet (sequences 17–22 and 25–29). This β-sheet has a right-handed twist as usual for such secondary structures. The β-turn connecting the two strands belongs to type II′. This structure is homologous to all scorpion toxin structures known so far as well as to insect defensins. The three arginines known to be involved in the pharmacological activity, i.e., Arg6, Arg7, and Arg13, are all located on the solvent-exposed side of the helix and form a positively charged surface which includes Gln9. The calculated electrostatic potential is highly asymmetric with the greatest positive potential centered on the Arg-rich α-helix side. Representation of the electrostatic fields by vectors revealed that the electrostatic potential and coherent field direction extended far out from the molecular surface. This suggests that local charge concentrations, rather than global charge, control productive recognition. The presence of the imidazole ring of His31 together with the presence of a C-terminal carboxyl amidation is necessary to obtain the irreversibility of the P05-NH_2 binding. This residue is remote from the positively charged surface, thus suggesting a multipoint interaction of P05-NH_2 with the receptor.

Peptide toxins found in animal venoms often act as neurotoxins by interacting with and modulating the activity of specific ion channels. Most of the scorpion toxins purified until now are active on the voltage-dependent sodium channel or excitable cells, either at the level of its inactivation or at the level of its activation (Cahalan, 1975; Catterall, 1980). Two types of toxins have been defined, α-toxins (site 3) and β-toxins (site 4), according to their binding to two different sites of the Na^+ channel of rat brain synaptosomes. Some of them are active on the mammal nervous system whereas others are specific for the insect nervous system (Couraud *et al.*, 1982; Zlotkin *et al.*, 1979). These toxins are 60–70 amino acid residues in length and are cross-linked by four disulfide bridges (Rochat *et al.*, 1979; Darbon *et al.*, 1982).

More recently, shorter scorpion neurotoxins have been purified that act on potassium channels: noxiustoxin (Possani *et al.*, 1982), charybdotoxin (Gimenez *et al.*, 1988), kaliotoxin

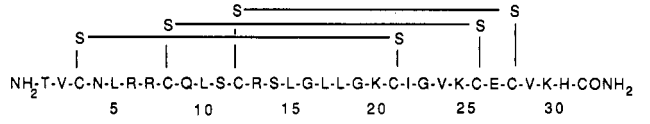

FIGURE 1: Amino acid sequence and disulfide pairing of P05-NH_2.

(Crest *et al.*, 1992), and iberotoxins (Galvez *et al.*, 1990). These toxins act on the voltage-dependent K^+ channels as well as on large conductance, calcium-activated potassium channels (maxi-K). Only leiurotoxin I acts on small-conductance calcium-dependent potassium channels. This channel is also called the apamin-sensitive potassium channel, since it is blocked by apamin, a neurotoxin isolated from bee venom. These neurotoxins are shorter (30–35 amino acid residue polypeptides) and reticulated by only three disulfide bridges. The venom of the scorpion *Androctonus mauretanicus mauretanicus* contains a toxin—P05—which is structurally and functionally similar to scorpion leiurotoxin I (87% sequence identity), a blocker of the apamin-sensitive Ca^{2+}-activated K^+ channels. P05, a 31-residue polypeptide cross-linked by three disulfide bridges (Zerrouk *et al.*, 1993), also possesses binding and physiological properties similar to those of the bee venom toxin apamin (18 residues, two disulfides).

‡ Twenty-five structure coordinates have been deposited in the Brookhaven Protein Data Bank under the file name 1PNH.

§ LCCMB, CNRS URA 1296.

‖ Sanofi-Recherche.

⊥ CNRS URA 1455.

• Abstract published in *Advance ACS Abstracts,* October 1, 1993.

0006-2960/93/0432-11969$04.00/0

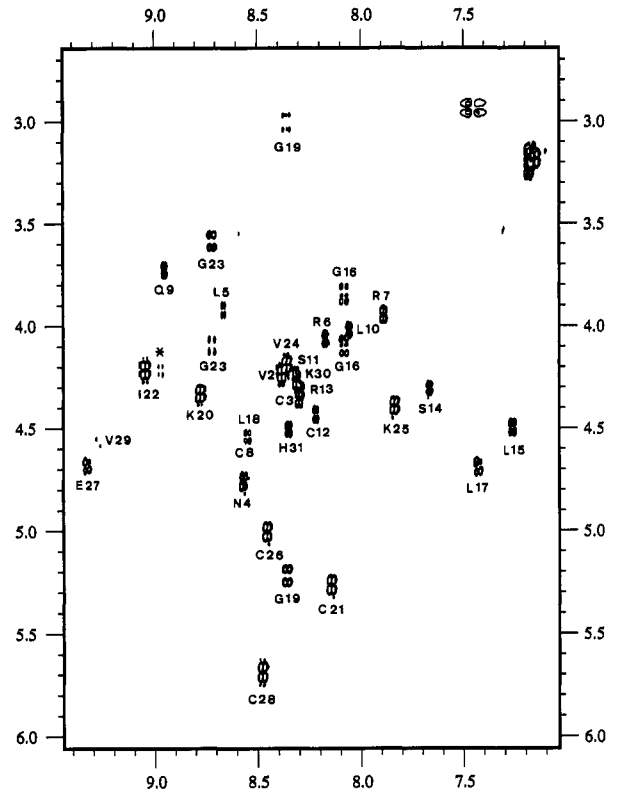

FIGURE 2: Contour plot of the fingerprint region of a DQF-COSY spectrum of P05-NH_2. The cross-peaks are labeled according to the sequential assignment. The star indicates the duplicated cross-peak of Ile22 corresponding to the cis conformation of the disulfide bridge linking Cys3 to Cys21.

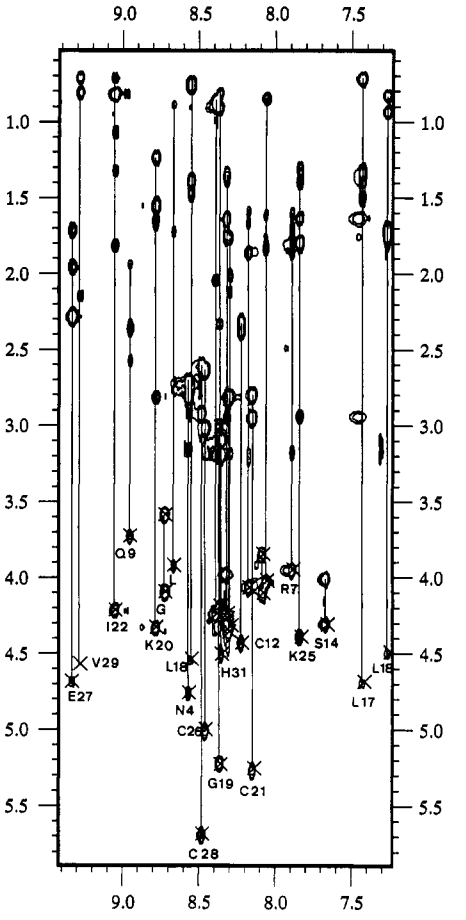

FIGURE 3: Contour plot of a TOCSY spectrum of P05-NH_2 with a spin-lock period of 100 ms. Spin systems are labeled with the sequential residue position and with a line connecting the NH–CαH cross-peak (labeled with a cross) with the side chain.

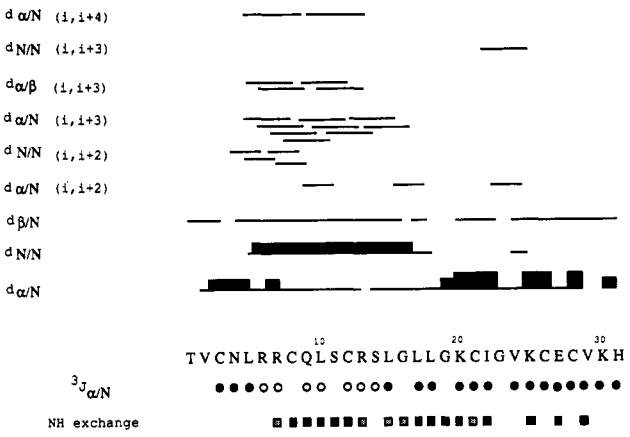

FIGURE 4: Summary of sequential and medium-range NOE's, $^3J_{HN\alpha}$, and amide proton exchange rates. Sequential NOE's are indicated with boxes whose size is proportional to the upper distance bound calculated from NOE intensity. Coupling constants $^3J_{HN\alpha}$ greater than 8 Hz are labeled with open circles and less than 7 Hz by closed circles. Low and intermediate amide proton exchange rates are indicated by closed boxes and open boxes, respectively.

However, the amino acid sequences of these two polypeptides are dissimilar, except for a common Arg-Arg-Cys-Gln motif which is located on an α-helix. Recently, we have reported both the chemical synthesis and biological characterization of a C-terminal carboxyl amidated analog of P05, termed sP05-NH_2 (Sabatier *et al.*, 1993). Synthetic sP05-NH_2, unlike native P05, was found to bind irreversibly to the apamin receptor, thus being an important pharmacological probe for the study of the small-conductance Ca^{2+}-activated K^+ channel (Figure 1). Further, structure–activity relationship studies using Arg-substituted analogs of sP05-NH_2 indicate that, as for apamin, Arg residues of the consensus motif are required in binding and expression of the leiurotoxin I/apamin-like biological properties of P05. Together, these data strongly suggest the importance of the common α-helical core for activity of this group of pharmacologically related toxins (P05-NH_2, apamin, leiurotoxin). Interestingly, extensive structure–activity relationship studies indicate that, for long scorpion toxins (60–70 residues, four disulfide bridges), the α-helical structure is not involved in pharmacological activity but more probably in stabilizing an active conformation of a solvent-exposed hydrophobic region (Darbon *et al.*, 1983; Kharrat *et al.*, 1989, 1990). In order to understand the precise molecular basis of the toxin to receptor recognition and for the rational design of new K^+ channel blockers, we report here the complete determination of the sP05-NH_2 three-dimensional structure by ^1H NMR and compare it with that of other ion channel blockers.

MATERIALS AND METHODS

Sample Preparation. Synthetic P05-NH_2 (sP05-NH_2) was obtained as previously described (Sabatier *et al.*, 1993). The toxin was dissolved to a final concentration of 5 mM in H_2O/D_2O (90/10, v/v). The pH was adjusted to 3.0 (uncorrected for isotope effect). For amide proton exchange experiments, the peptide was lyophilized and redissolved in D_2O and then immediately inserted into the preshimmed spectrometer.

NMR Spectroscopy. Proton NMR spectra were routinely recorded at 37 °C on a Bruker AMX500 spectrometer. A double-quantum-filtered 2-D correlation spectrum (DQF-

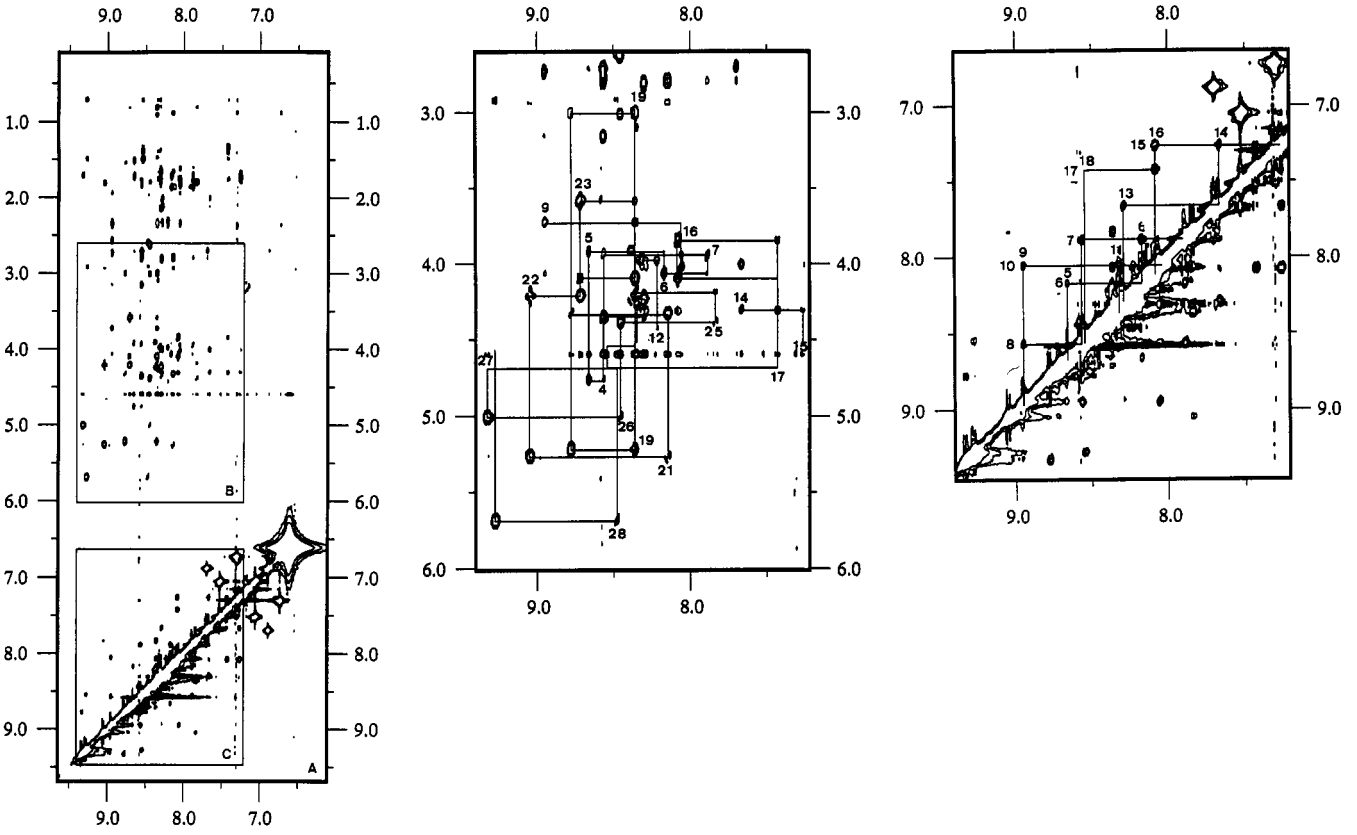

FIGURE 5: NOESY spectrum recorded with 100-ms mixing time. (A, left) Overview of the amide proton region. The regions of interest for sequential assignment are boxed. (B, middle) Contour plot of the fingerprint region. The sequential $d_{\alpha N}$ connectivities are illustrated by lines. Some COSY NH–CαH cross-peaks are labeled according to the sequential assignment. (C, right) Contour plot of the amide region. The sequential d_{NN} connectivities are illustrated by lines.

COSY) (Piantini *et al.*, 1982) was acquired in the phase-sensitive mode by time-proportional phase incrementation of the first pulse (TPPI) (Marion & Wüthrich, 1983). A clean total correlation spectrum (CLTOCSY) was acquired with a mixing time of 100 ms using TPPI. A phase-sensitive 2-D nuclear Overhauser effect (NOE) spectrum (NOESY) (Jeener *et al.*, 1979; Kumar *et al.*, 1981) was acquired using TPPI with mixing times of 100 ms. The solvent OH resonance was suppressed by low-power irradiation during the relaxation delay and, for NOESY, during the mixing time.

After the two-dimensional data matrices were zero-filled to 2K in both dimensions (800 experiments were typically recorded with 1K data points) and multiplied by a shifted sine-bell window in both dimensions, two-dimensional spectra were Fourier transformed and baseline corrected with standard Bruker UXNMR software, running on X32 station, and FTTOOL software (Eccles, personal communication), running on an IRIS 4D-380 Silicon Graphics computer. After zero filling, the digital resolution was 3.2 Hz/point in both dimensions.

Identification of the amino acid spin systems and sequential assignment were achieved using the well-known general strategy described by Wüthrich (1986) and gave rise to a full proton assignment. Identification of spin systems was obtained by analysis and comparison of 2-D DQF-COSY and CLTOCSY recorded in water.

Stereospecific assignments for β-methylene protons were made by analysis of the $^3J_{\alpha\beta}$ and the intraresidue NH–β and α–β NOE's. In this way, 9 of the 14 nondegenerated β-methylene protons were assigned using the program HABAS (Güntert *et al.*, 1991).

NOE intensities, used as input for the structure calculations, were obtained from a NOESY spectrum recorded with a 100-ms mixing time on the fully protonated sample, and the peaks were integrated by the peak-integration routine of the EASY software (Eccles *et al.*, 1991), running on an IPC SUN station. Buildup curves obtained by integrating NOE peaks from NOESY recorded with 100-, 200-, and 300-ms mixing times show that no spin diffusion occurs below 250 ms. Most of the NOE cross-peaks were unambiguously assigned on the basis of their unique chemical shifts due to the great dispersion of the signals. The intraresidual and sequential NOE's were partitioned into four categories (strong, medium, weak, and very weak) that were converted into distance restraints (<2.4, <2.9, <3.5, and <5.0 Å, respectively) using a calibration curve based on known distances; i.e., $d_{\alpha\alpha}$ = 2.3 Å between two strands of antiparallel β-sheet, d_{NN} (i,i+1 in α-helix) = 2.8 Å, d_{NN} = 3.3 Å between two strands of antiparallel β-sheet, $d_{\alpha N}$ (i,i+3 in α-helix) = 3.4 Å, and $d_{\alpha N}$ (i,i+4 in α-helix) = 4.2 Å. The calibration curve was obtained after averaging the volume of all resolved peaks used for the calibration. The medium-range and long-range NOE's were then converted into <4- or <5-Å distance restraints, depending on whether or not they occur between two backbone protons. Pseudoatom corrections were added when no stereospecific assignments were available (Wüthrich, 1986). Lower distance restraints were systematically set to 1.8 Å.

Amide protons exhibiting low rates of exchange with the solvent were identified following dissolution in D_2O. Immediately after dissolution, a series of short (10-h) 100-ms NOESY spectra were recorded. Amide protons still giving rise to off-diagnonal signals 90 h after dissolution of the sample were then considered to be slowly exchangeable. Off-diagonal signals disappearing after 50 h were considered as belonging to intermediate exchange rate amide protons.

Table I: ^{1}H Chemical Shifts for P05 at 310 K, pH 3.0, Taking the Water Resonance as Reference (4.6 ppm)[a]

residue	NH	αH	βH	others
Thr1		4.06	3.92	CγH_3 1.27
Val2	8.38	4.24	2.04	CγH_3 0.89, 0.86
Cys3	8.30	4.35	2.81, 2.81	
Asn4	8.56	4.76	2.81*, 2.70	NH_2 7.70, 6.88
Leu5	8.66	3.93	1.72*, 1.51	CγH 1.40, CδH_3 0.89
Arg6	8.17	4.07	1.86	CγH 1.67, 1.59; CδH 3.24, 3.18; NH_2 7.18
Arg7	7.89	3.95	1.85, 1.79	CγH, 1.70, 1.60; CδH 3.18; NH_2 7.17
Cys8	8.56	4.57	3.16, 2.74	
Gln9	8.95	3.73	2.36, 1.95*	CγH 2.58; NH_2 7.30, 6.72
Leu10	8.06	4.03	1.83, 1.61	CγH 1.77; CδH_3 0.85
Ser11	8.32	4.23	3.98, 3.98	
Cys12	8.22	4.44	2.38, 2.31*	
Arg13	8.29	4.31	2.12, 2.01*	CγH 1.76; CδH 3.18; NH_2 7.15
Ser14	7.67	4.31	4.01, 4.01	
Leu15	7.26	4.50	1.75, 1.75	CγH 1.75; CδH_3 0.93, 0.83
Gly16	8.08	4.10, 3.86		
Leu17	7.43	4.68	1.32, 1.32	CγH 1.49; CδH_3 0.72
Leu18	8.54	4.54	1.47*, 1.39	CγH 1.39; CδH_3 0.78, 0.73
Gly19	8.36	5.22, 3.01		
Lys20	8.78	4.34	1.65, 1.65	CγH 1.24; CδH 1.56; CεH 2.82; NH_2 6.87
Cys21	8.14	5.27	2.95, 2.80*	
Ile22	9.05	4.22	1.81	CγH 1.32, 1.07; CγH_3 0.82; CδH_3 0.72
Gly23	8.72	4.10, 3.59		
Val24	8.36	4.19	2.33	CγH_3 0.91, 0.81
Lys25	7.84	4.39	1.80, 1.80	CγH 1.40, 1.32; CδH 1.63; CεH 2.94; NH_2 7.46
Cys 26	8.45	5.01	3.02, 2.63*	
Glu27	9.33	4.67	1.97, 1.71	CγH 2.28
Cys28	8.48	5.69	2.93, 2.61*	
Val29	9.28	4.57	2.15	CγH_3 0.81, 0.71
Lys30	8.31	4.27	1.75, 1.75	CγH 1.36; CδH 1.64; CεH 2.94; NH_2 7.46
His31	8.35	4.51	3.19, 3.11	

[a] An asterisk indicates the βH_2 proton when the βCH methylene has been stereospecifically assigned.

Measurement of the spin coupling constants, $^3J_{HN\alpha}$, was done on cross sections parallel to F_2 through NH–CαH of a DQF-COSY obtained after zero filling to 8K in F_2. Still, the low resolution of such a spectrum prevented us from getting accurate $^3J_{HN\alpha}$. The coupling constants were thus divided into small (<7 Hz) and large (>8 Hz) and translated into −40°/−80° and −70°/−160° angle restraints, respectively.

The final set of restraints obtained after the ineffective restraints were removed, consisted of 94 intraresidue, 67 sequential, 34 medium-range, and 27 long-range distance restraints, as well as 25 angle restraints and 12 hydrogen bonds.

Structure Calculations. Distance geometry calculations were performed with the DIANA package (Güntert *et al.*, 1991).

A total of 1000 DIANA structures with randomly generated starting conformations were initiated. The first round of calculation included only intraresidual and sequential restraints. The 500 best solutions as judged from the residual constraint violations were then calculated using distances extracted from medium-range NOE's. Finally, 250 structures were obtained using the whole set of distance constraints. These 250 best structures, as judged from the residual violations and the value of the target function, were used as starting structures in another DIANA calculation, including the distance data obtained from amide proton exchange experiments. The d_{CO-HN} constraint was set to 2.5 Å when the hydrogen bond partners were obviously identified on the basis of the visual analysis of the structures previously obtained. In a last round of calculations, the angle constraints derived from the $^3J_{HN\alpha}$ coupling constants were added.

These 25 best structures were then energy minimized over 10 000 iterations of the Powell minimizer using the molecular dynamics software XPLOR (Brünger, 1990), including the whole set of NMR restraints.

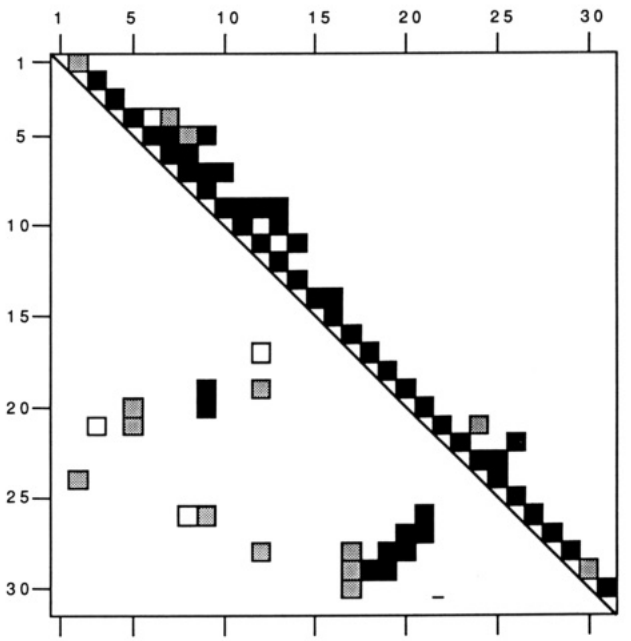

FIGURE 6: Summary of NOE data. Sequential and medium-range NOE's are indicated above the diagonal, and long-range NOE's are indicated below the diagonal. A filled square indicates that an NOE between two backbone atoms is detected. A shaded square indicates that the detected NOE involves only one backbone atom. An open square indicates that both partners are side-chain protons. When more than one NOE is detected between two residues, only the one involving the highest number of backbone atoms is indicated.

DIANA and XPLOR calculations were done on an IRIS 4D-380 VGX Silicon Graphics computer. Visual analysis and RMSD calculations of the obtained structures were done with the TURBO-FRODO program (Roussel & Cambillau, 1989), running on an IRIS 4D-380 VGX Silicon Graphics computer.

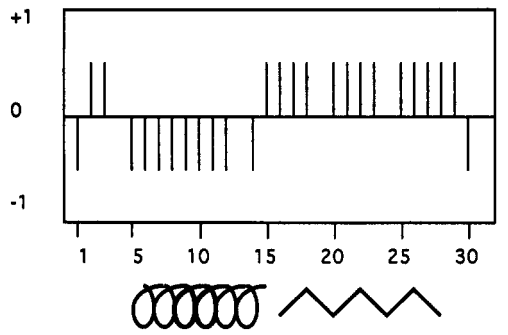

FIGURE 7: Assignment of secondary structure of P05-NH_2 as determined by the chemical shift index method. The observed CαH chemical shifts are compared with the random coil values given by Wüthrich (1986). A 1, a 0, or a −1 value shows respectively that the backbone α-proton chemical shift of a given residue is above, within, or below the range given by Wishart *et al.* (1992). Any dense grouping of four or more 1's not interrupted by a −1 is a β-strand. Any dense grouping of four or more −1's not interrupted by a 1 is an α-helix.

RESULTS

Sequential Assignment. The sequence assignment of resonances was performed using the now conventional procedures (Wüthrich, 1986). Cross-peaks between NH and CαH were identified by examination of the DQF-COSY spectrum (Figure 2). Spin systems were identified on the basis of DQF-COSY, and the CLTOCSY spectrum was used to correlate these side-chain spin systems with the NH–CαH cross-peaks (Figure 3). Intraresidue NOESY cross-peaks were used to discriminate between aspartate/asparagine and glutamate/glutamine, respectively. The CLTOCSY spectrum allowed us to assign methyl groups of leucine and isoleucine.

The sequential assignment (Figure 4) was then achieved by virtue of $d_{\alpha N}$, d_{NN}, and $d_{\beta N}$ connectivities (Figure 5). The glycine, valine, threonine, and serine which were assigned as amino acid cross-peaks rather than by spin system class were particularly useful in identifying stretches of adjacent residues. The so-obtained resonance assignments are listed in Table I with the exception of NH of Thr 1, for which no NH–CαH cross-peak could be identified, due probably to the rapid exchange of the NH_3^+ at this pH.

Secondary Structure. The analysis of the secondary structure of P05-NH_2 was based on the data summarized in Figures 5 and 6. As can be seen from Figure 4, the pattern of d_{NN}, $d_{\alpha N}$ $(i,i+3)$, and $d_{\alpha\beta}$ $(i,i+3)$ suggests a helix running from residues 5 to 17. This is confirmed at least up to residue 14 by the small $^3J_{HN\alpha}$ values (25 coupling constants were determined) and the NH exchange rate. The $d_{\alpha N}$ $(i,i+4)$ (althrough there are few) are indicative of an α-type helix.

The pattern of NOE's seen in the residue 19–29 region together with large $^3J_{HN\alpha}$ values and long-range NOE's (Figure 6) is consistent with a sheet made of two antiparallel β-strands connected by a turn centered on residues 23 and 24. This antiparallel β-sheet is further confirmed by the slow HN exchange rate observed for all protons expected to be involved in hydrogen bonds. This secondary structure found is confirmed by the results of the chemical shift index method of Wishart *et al.* (1992) (Figure 7) and is in complete accordance with the secondary structure determination of the homologous scorpion toxin leiurustoxin I (Auguste *et al.*, 1990).

Structure Calculation by Distance Geometry and Refinement by Molecular Dynamics. The final step of calculation, including the whole set of constraints, i.e., 94 intraresidue, 67 sequential, 34 medium-range $(d < i,i+5)$, and 27 long-range distance restraints as well as 25 angle restraints and 12 hydrogen bonds, led to 250 structures from which the 25 best, as judged from residual violation of the restraints, were kept for analysis and refinement. A summary of the structural statistics for the obtained structures is presented in Table II. The overall agreement among the different structures can be summarized by RMSD values. Calculated as an average of RMSD's of all pairwise combinations of the 25 structures obtained by distance geometry, the RMSD for backbone atoms is 0.98 Å. This value drops to 0.83 Å if we discard residues 1, 2, 30, and 31. The data demonstrate that the structure of P05-NH_2 is well-defined between Cys3 and Val29, the N- and C-ends being less constrained. Residues excluded from these statistics, i.e., Thr1, Val2, Lys30, and His31, are thus considered as disordered as far as the NMR data are concerned. All of the 25 structures are equally compatible with the set of restraints as no violation of distance larger than 0.25 Å is found. Furthermore, the average violation is low (0.002 Å).

DISCUSSION

Analysis of the Final Structure. Figure 8 shows a superposition of the 25 best structures resulting from distance

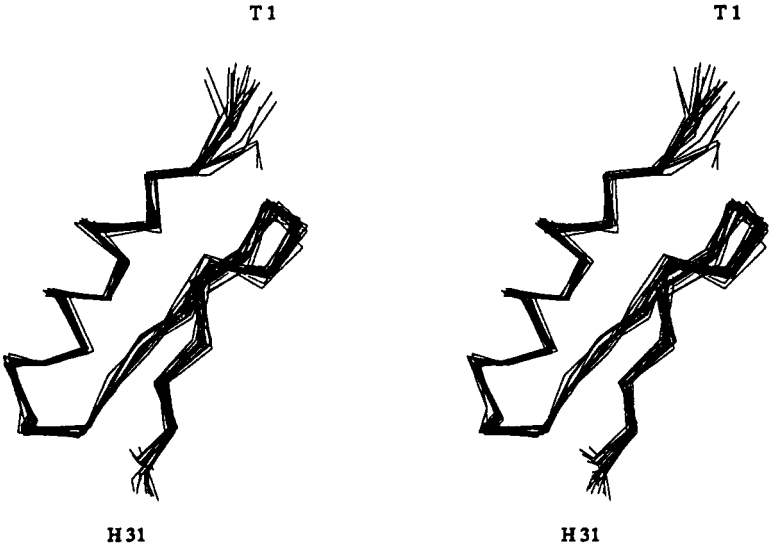

FIGURE 8: Stereoview of the 25 best molecular P05-NH_2 structures (only Cα atoms are displayed) superimposed for best fit on backbone heavy atoms.

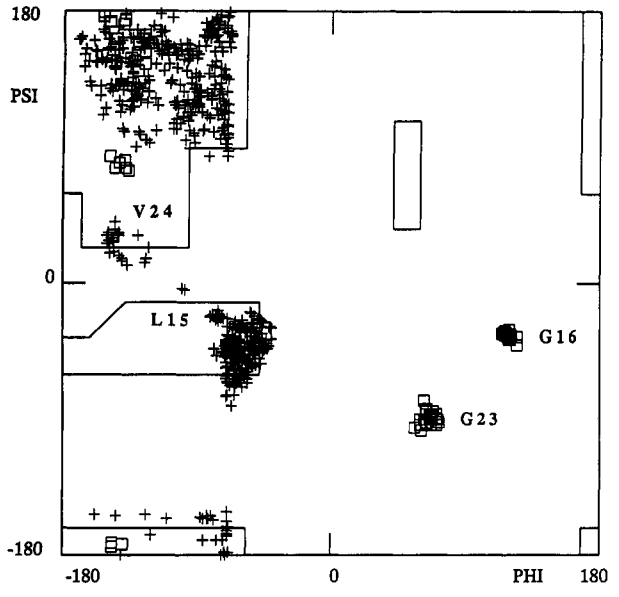

FIGURE 9: Ramachandran plot for the 25 best structures.

Table II: Structural Statistics for 25 Structures

av no. of violations >0.2 Å	0.68
av violation (Å)	0.051
av energies (kcal/mol)	
electrostatic	−951
dihedrals	44
bonds	6
angles	44
van der Waals	−85
impropers	6
total	−936
RMSD[a]	
residues 1–31	0.98
residues 3–29	0.83

[a] RMSD refers to root mean square differences calculated on backbone residues.

geometry followed by energy minimization. The RMSD to the mean structure is 0.64 for backbone atoms, indicating a good definition of the backbone. This value rises to 1.436 if we include all non-hydrogen atoms. This indicates that the side chains are poorly defined, because most of them are immersed in the solvent. The relatively low number of distance restraints used in the calculation (7.5 restraints/residue) still gives rise to well-defined structures because most of them involve backbone or β-protons.

P05-NH_2 has a globular structure consisting of an α-helix (residues 5–14) connected by a tight turn to a two-stranded antiparallel β-sheet (sequences 17–22 and 25–29). This β-sheet is right-hand twisted as usual for such secondary structures, stabilized by six hydrogen bonds involving the 18/29, 20/27, 22/25, 25/22, 27/20, and 29/18 HN/CO couples. The tight turn connecting the α-helix to the first strand of β-sheet is stabilized by two hydrogen bonds involving the amide protons of residues 16 and 17 on one hand and the carbonyl oxygen of residue 12 on the other hand.

The Ramachandran plot shown in Figure 9 indicates that the geometry of the calculated solutions is good. This plot shows usual angles for β-sheets and α-helix. The ϕ,ψ angle couples of residue 24 are compatible with a type II′ running from residue 22 to residue 25, according to the classification of Richardson (1981) in which the second residue is usually a glycine (here Gly23).

Disulfide Bridges. The disulfide pairing was previously chemically determined (Sabatier *et al.*, 1993) and used as input for the structure calculations. The three disulfide bonds, i.e., 3–21, 8–26, and 12–28, hold the α-helix in proximity to the β-sheet. During resonance assignment, a few CαH–NH peaks were found to be split, due to slightly different NH chemical shifts. These split peaks belong to Cys residues as well as some adjacent residues, i.e., Arg7, Cys8, Gln9, Cys12, Lys20, Cys21, Ile22, and Cys28. The splitting most probably arises from the existence of a minor conformation of these disulfide bridges. Such an isomerization has been recently described for CsE V3 scorpion toxin (Zhao *et al.*, 1992). These authors refined this structure to high resolution and interpreted an additional electron density in terms of disulfide bridge isomerization instead of water molecules as previously proposed for lower resolution structures.

In our NMR spectra, the low intensity of the additional cross-peaks coming from the minor conformations indicates that these conformations represent less than 10% of the population and were thus not considered during structure computations. Furthermore, no other splittings were found in the spectra, demonstrating that the overall structure of P05-NH_2 is not altered by such an isomerization.

The proximity of disulfide bridges 8/26 and 12/28 induces a deshielding effect on neighboring protons, clearly demonstrated by the downfield shift of α-protons of Gly19, Cys21, Cys26, and Cys28 (Table I).

Comparison of the P05-NH_2 Structure with Other Scorpion Toxins. The structures of some scorpion toxins have been described over the past years. They can be divided into "long" scorpion toxins (60–70 amino acid residues and four disulfide bridges) and "short" scorpion toxins (30–37 amino acid residues and three disulfide bridges). These molecules, although they have various modes of action and different target receptors, share a common structural motif, consisting of a β-sheet connected to an α-helix by three disulfide bridges. Two of these bridges connect the Cys-X-X-X-Cys sequence in the helix to the Cys-X-Cys sequence in a strand. The third bridge is less constant although always connecting the

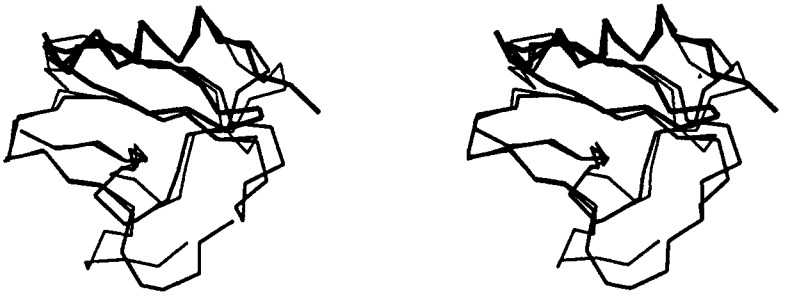

FIGURE 10: Superposition of P05-NH_2 (heavy line) with long scorpion toxin X-ray structures: CsE V3 (thin lines; Fontecilla-Camps *et al.*, 1980); AaHII (medium lines; Fontecilla-Camps *et al.*, 1988).

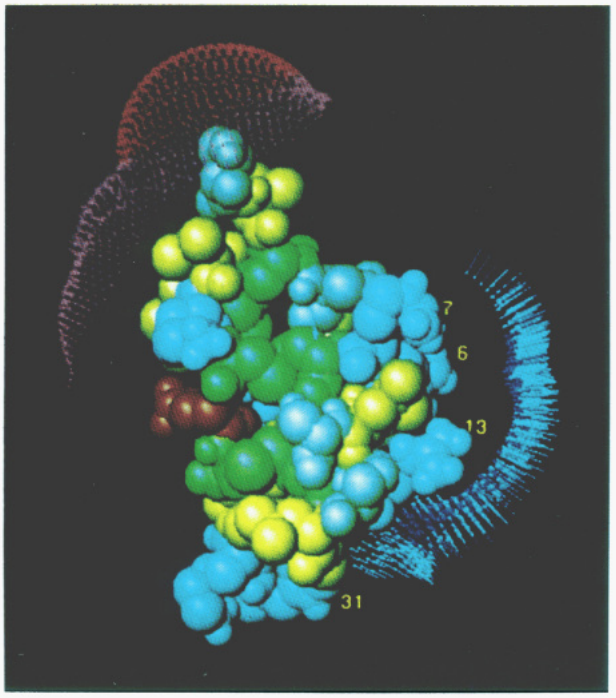

FIGURE 11: Space-filling model of one P05-NH_2 structure. The structure is colored according to the type of amino acid residue, with positive residues in blue, negative residues in red, cystines in dark green, aliphatic residues in yellow, and all others in light green. The arrows representing the electrostatic field vectors are color-coded according to the magnitude of the field (red < pink < light blue < dark blue).

beginning of the helix to the upper strand of the β-sheet (Fontecilla-Camps *et al.*, 1980, 1988; Martins *et al.*, 1990; Bontemps *et al.*, 1991; Darbon *et al.*, 1991).

P05-NH_2 also possesses this motif and can easily be superimposed on long scorpion toxins (Figure 10), and also on short scorpion toxins, such as charybdotoxin or iberotoxin (not shown). Interestingly, the common structural motif is also present in insect defensins (Bontems *et al.* 1991), a molecule with an antibacterial activity in insects and in thionins from the endosperm of several Gramineae (Bruix *et al.*, 1993). These last two molecules have the same cystine pattern as scorpion toxins.

Structure–Activity Relationships. Despite their structural homologies, scorpion toxins have very different modes of action. P05-NH_2 and the highly homologous leiurotoxin I (Auguste *et al.*, 1990) act as blockers of the small-conductance calcium-activated potassium channel in various cell types (Abia *et al.*, 1986; Chicchi *et al.*, 1988; Castle *et al.*, 1986) and have been shown to possess binding and physiological properties similar to those of apamin purified from bee venom, although these toxins do not share any striking sequence homology.

An analog of P05-NH_2, in which Arg6 and Arg7 were replaced by leucines, was shown to be inactive in vivo when injected into mice and to possess 1/5000 of the activity of native P05-NH_2 when tested for its ability to compete with ^{125}I-labeled apamin for binding to synaptosomes (Sabatier *et al.*, 1993). Replacing these two arginines by lysine induced only a 10-fold decrease of activity. In addition, Martins *et al.* (1990) have proposed that Arg13 of leiurotoxin I is also involved in the binding to the receptor. Structure–activity relationship studies of apamin have shown that two contiguous arginines, i.e., Arg13 and Arg14, as well as Gln16, all located on an α-helix, are necessary for binding activity of this molecule (Labbé-Julié *et al.*, 1991). On the contrary, long scorpion toxins are believed to interact with their receptor sites located on the voltage-dependent Na^+ channel via a solvent-exposed hydrophobic surface.

Figure 11 shows a space-filling representation of P05-NH_2 together with the electrostatic field calculated according to Roberts *et al.* (1991) (Roussel and Cambillau, personal communication). The three arginines, i.e., Arg6, Arg7, and Arg13, all located on the solvent-exposed side of the helix which is believed to interact with the receptor, form a positively charged surface which includes Gln9. The calculated electrostatic potential is highly asymmetric, with the greatest positive potential centered on Gln9. Representation of the electrostatic fields by vectors revealed that the electrostatic potential and coherent field direction extended far out the molecular surface of the peptide. This suggests that local charge density, rather than global charge, controls productive recognition.

The presence of the imidazole ring of His31 together with the C-terminal carboxyl amidation is necessary to obtain the irreversibility of the P05-NH_2 binding. This residue is remote from the positively charged surface, thus suggesting a multipoint interaction of P05-NH_2 with the receptor. The position of the side chain of the C-terminal histidine cannot be determined with accuracy, due to the lack of NMR restraints for this residue. However, from Figure 12, where the P05-NH_2 structure is shown with the α-helix axis perpendicular to the picture, one can postulate that the imidazole ring can be part of the interaction.

Structure determination of inactive analogs is under way and will allow a better understanding of the binding activity of this potent marker of the small-conductance calcium-activated potassium channel.

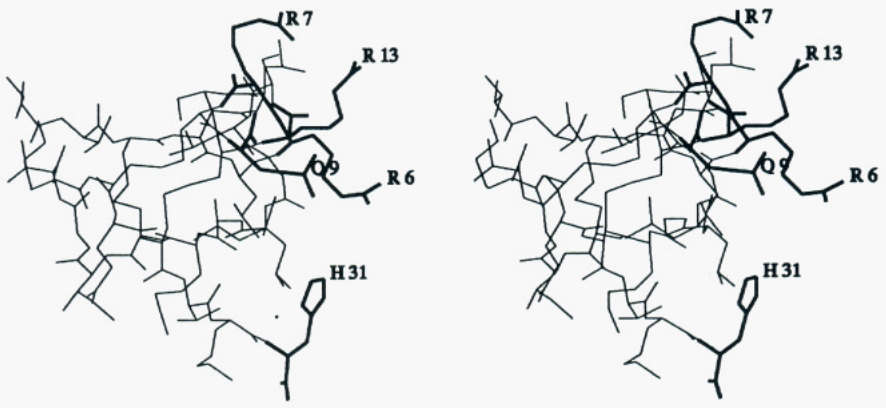

FIGURE 12: Stereoview of one P05-NH_2 structure oriented so that the α-helix axis is perpendicular to the plane of the paper. Residues of interest for pharmacological properties of the molecule are in heavy lines.

REFERENCES

Abia, A., Lobaton, C. D., Moreno, A., & Garcia-Sancho, J. (1986) *Biochim. Biophys. Acta 856*, 403–407.

Auguste, P., Hugues, M., Gravé, B., Gesquiere, J. C., Maes, P., Tartar, A., Romae, G., Schweitz, H., & Lazdunski, M. (1990) *J. Biol. Chem. 265*, 4753–4759.

Bontems, F., Roumestand, C., Gilquin, B., Ménez, A., & Toma, F. (1991) *Science 254*, 1521–1523.

Bruix, M., Jiménez, M. A., Santoro, J., Gonzales, C., Colilla, F. J., Mendez, E., & Rico, M. (1993) *Biochemistry 32*, 715–724.

Brünger, A. T. (1990) *X-PLOR v2.1 Manual*, Yale University, New Haven, CT.

Cahalan, M. D. (1975) *J. Physiol. 244*, 511–534.

Castle, N. A., & Strong, P. N. (1986) *FEBS Lett. 209*, 117–121.

Catterall, W. A. (1980) *Annu. Rev. Pharmacol. Toxicol. 20*, 15–43.

Chicchi, G. G., Gimenez-Gallego, G., Ber, E., Gargia, M. L., Winquist, R., & Cascieri, M. A. (1988) *J. Mol. Biol. 263*, 10192–10197.

Couraud, F., Jover, E., Dubois, J. M., & Rochat, H. (1982) *Toxicon 20*, 9–16.

Crest, M., Jacquet, G., Gola, M., Zerrouk, H., Benslimane, A., Rochat, H., Mansuelle, P., & Martin-Eauclaire, M. F. (1992) *J. Biol. Chem. 267*, 1640–1647.

Darbon, H., Zlotkin, E., Kopeyan, C., Van Rietchoten, J., & Rochat, H. (1982) *Int. J. Pept. Protein Res. 20*, 320–330.

Darbon, H., Jover, E., Couraud, F., & Rochat, H. (1983) *Int. J. Pept. Protein Res. 22*, 179–186.

Darbon, H., Weber, C., & Braun, W. (1991) *Biochemistry 30*, 1836–1844.

Eccles, C., Güntert, P., Billeter, M., & Wüthrich, K. (1991) *J. Biomol. NMR 1*, 111–130.

Fontecilla-Camps, J. C., Almassy, R. J., Suddath, F. L., Watt, D. D., & Bugg, C. (1980) *Proc. Natl. Acad. Sci. U.S.A. 77*, 6496–6500.

Fontecilla-Camps, J. C., Habetsetzer-Rochat, C., & Rochat, H. (1988) *Proc. Natl. Acad. Sci. U.S.A. 85*, 7443–7447.

Galvez, A., Gimenez, G., Reuben, J. P., Ray-Contanain, L., Feigenbaum, P., Kaczorowski, G. J., & Garcia, M. L. (1990) *J. Biol. Chem. 265*, 11083–11090.

Garcia, M. L., Galvez, A., Garcia-Calvo, M., King, F., Vasquez, J., & Kaczorowski, G. L. (1991) *J. Bioenerg. Biomembr. 23*, 615–645.

Gimenez, G., Navia, M. A., Reuben, J. P., Katz, G. M., Kaczorowshi, G. J., & Garcia, M. L. (1988) *Proc. Natl. Acad. Sci. U.S.A. 85*, 3329–3333.

Güntert, P., Braun, W., & Wüthrich, K. (1991) *J. Mol. Biol. 217*, 517–530.

Jeener, J., Meier, B. H., Bachmann, P., & Ernst, R. R. (1979) *J. Chem. Phys. 71*, 4546–4553.

Kharrat, R., Darbon, H., Rochat, H., & Granier, C. (1989) *Eur. J. Biochem. 181*, 381–390.

Kharrat, R., Darbon, H., Granier, C., & Rochat, H. (1990) *Toxicon 28*, 509–523.

Kumar, A., Ernst, R. R., & Wüthrich, K. (1981) *Biochem. Biophys. Res. Commun. 95*, 1–6.

Labbé-Julié, C., Granier, C., Albericio, F., Defendini, M.-L., Ceard, B., Rochat, H., & Van Rietschoten, J. (1991) *Eur. J. Biochem. 196*, 639–645.

Marion, D., & Wüthrich, K. (1983) *Biochem. Biophys. Res. Commun. 113*, 967–974.

Martins, J. C., Zang, W., Tartar, A., Lazdunski, M., & Borremans, F. A. M. (1990) *FEBS Lett. 260*, 249–253.

Piantini, U., Sorensen, O. W., & Ernst, R. R. (1982) *J. Am. Chem. Soc., 104*, 6800–6801.

Possani, L. D., Martin, B. M., & Svendsen, I. (1982) *Carlsberg Res. Commun. 47*, 285–289.

Richardson, J. S. (1981) *Adv. Protein Chem. 34*, 167–339.

Roberts, V. A., Freeman, H. C., Olson, A. J., Tainer, J. A., & Getzoff, E. D. (1991) *J. Biol. Chem. 266*, 13431–13441.

Rochat, H., Bernard, P., & Couraud, F. (1979) *Adv. Cytopharmacol. 3*, 325–334

Roussel, A., & Cambillau, C. (1989) in *Silicon Graphics Geometry Partner Directory (Fall 1989)* (Silicon Graphics, Ed.) pp 77–78, Silicon Graphics, Mountain View, CA.

Sabatier, J. M., Zerrouk, H., Darbon, H., Mabrouk, K., Benslimane, A., Rochat, H., Martin-Eauclaire, M.-F., & Van Rietschoten, J. (1993) *Biochemistry 32*, 2763–2770.

Wishart, D. S., Sykes, B. D., & Richards, F. M. (1992) *Biochemistry 31*, 1647–1651.

Wüthrich, K. (1986) *NMR of Protein and Nucleic Acid*, John Wiley and Sons, New York.

Zerrouk, H., Mansuelle, P., Benslimane, A., Rochat, H., & Martin-Eauclaire, M. F. (1993) *FEBS Lett.* (in press).

Zhao, G., Carson, M., Ealick, S. E., & Bugg, C. E. (1992) *J. Mol. Biol. 227*, 239–252.

Zlotkin, E., Teitelbaum, Z., Rochat, H., & Miranda, F. (1979) *Insect Biochem. 9*, 347–354.